

# First-principles study of improper ferroelectricity in $\text{TbMnO}_3$

Andrei Malashevich\* and David Vanderbilt

*Department of Physics & Astronomy, Rutgers University, Piscataway, NJ 08854-8019, USA*

(Dated: August 22, 2021)

We have carried out a first-principles theoretical study of the magnetically induced polarization in orthorhombic  $\text{TbMnO}_3$ , a prototypical material in which a cycloidal spin structure generates an electric polarization via the spin-orbit interaction. We compute both the electronic and the lattice-mediated contributions to the polarization and find that the latter is strongly dominant. We analyze the spin-orbit induced forces and lattice displacements from both atomic and mode-decomposition viewpoints, and show that a simple model based on nearest Mn–Mn neighbor Dzyaloshinskii-Moriya interactions is not able to account fully for the results. The direction and magnitude of our computed polarization are in good agreement with experiment.

PACS numbers: 75.80.+q, 77.80.-e

Multiferroic and magnetoelectric materials are currently under intensive study, both from the point of view of fundamental materials physics and because of their potential application in novel technological devices such as memories, sensors, and transducers [1]. An interesting class of systems are “improper ferroelectrics” in which the magnetic order induces an electric polarization in a material that is otherwise structurally centrosymmetric. This can happen in collinear spin systems if the spin pattern breaks inversion symmetry; examples include  $RMn_2O_5$  ( $R=\text{Tb}, \text{Y}, \text{etc.}$ ) [2, 3], the E phase of orthorhombic  $RMnO_3$  ( $R=\text{Ho}, \text{Tb}$ ) [4, 5],  $\text{TbMnO}_3$  in magnetic field [6], and  $\text{Ca}_3\text{Co}_{2-x}\text{Mn}_x\text{O}_6$  [7]. In such cases, symmetric exchange interactions can explain the development of polar order, i.e., via exchange striction effects [5, 8]. Here we shall be concerned with another class of systems in which a non-collinear cycloidal spin structure induces an electric polarization via the spin-orbit (SO) interaction [9]; examples include  $\text{Ni}_3\text{V}_2\text{O}_8$  [10],  $\text{CuFeO}_2$  [11], and orthorhombic  $RMnO_3$  ( $R=\text{Tb}, \text{Dy}, \text{Ho}, \text{etc.}$ ) [12, 13, 14]. While such spiral spin structures and the resulting polarizations usually appear only at low temperature, these systems are of special interest because the coupling between magnetic and electric degrees of freedom is so profound.

Theoretically, symmetry analysis and phenomenological models have clarified the circumstances under which a spiral spin structure can give rise to an electric polarization [15, 16, 17], but are not well suited to identifying the dominant microscopic mechanism responsible for the polar order. Microscopic models have been introduced and used to discuss possible mechanisms, which can be divided broadly into two categories. The first are purely electronic mechanisms, in which the SO interaction (SOI) modifies the hybridization of electronic orbitals in such a way as to shift the center of charge [18, 19, 20, 21]. The second are “lattice mechanisms” involving magnetically-induced ionic displacements, usually discussed in terms of Dzyaloshinskii-Moriya (DM) interactions [17, 22, 23]. However, it is generally difficult to estimate the magni-

tudes (and even signs) of these two kinds of contributions from the models. Because experiments have not been sensitive enough to resolve the tiny SO-induced atomic displacements, a central unanswered question is whether electronic or lattice mechanisms are dominant. It is also unclear whether the pattern of displacements should follow the predictions of a simple DM model, or whether more complicated interactions enter the picture.

First-principles calculations can play an invaluable role in resolving such questions. Density-functional theory (DFT) has proven to be an extremely useful tool in understanding the physics of ordinary ferroelectric materials, and has already been used to make important contributions to the understanding of improper magnetic ferroelectrics of the collinear-spin type [24, 25, 26] and in the spiral magnetic materials  $\text{LiCu}_2\text{O}_2$  and  $\text{LiCuVO}_4$  [27]. However, to our knowledge such methods have not previously been applied to study the cycloidal magnetic states in the orthorhombic perovskite system.

In this Letter, we choose orthorhombic  $\text{TbMnO}_3$  as a paradigmatic system of the cycloidal type, and carry out a detailed first-principles study of the mechanisms by which the cycloidal magnetic order gives rise to the polarization. We demonstrate that DFT calculations predict the appearance of electric polarization in the cycloidal state via two mechanisms, a purely electronic one and a lattice-mediated one, and that the latter is strongly dominant. Nevertheless, we find that the DM theory alone cannot explain the computed pattern of atomic displacements, suggesting that other interactions not included in simple DM models play an important role.

Ferroelectricity coupled to spiral magnetic order was discovered in the orthorhombic perovskite  $\text{TbMnO}_3$  (space group  $Pbnm$ ) [12] with a 20-atom cell containing four formula units. The  $\text{Mn}^{3+}$  ions form a collinear sinusoidal spin wave at temperatures between  $\sim 27$  K and  $\sim 41$  K, but below  $\sim 27$  K a cycloidal spin wave forms with incommensurate wavevector  $k_s \sim 0.28$  along  $b$ , and a polarization simultaneously appears along  $c$  [9, 12].

In this work, electronic-structure calculations are car-

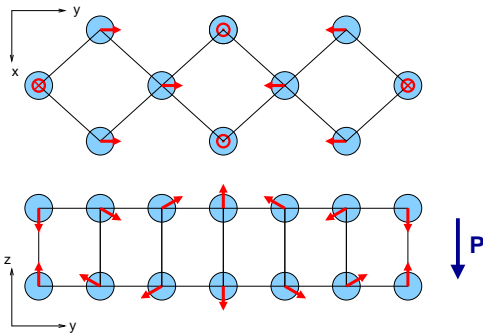


FIG. 1: (Color online) Sketch of  $a \times 3b \times c/2$  orthorhombic cell of  $\text{TbMnO}_3$  ( $Pbnm$  space group) showing  $\text{Mn}^{3+}$  sites with a cycloidal magnetic structure.

ried out using a plane-wave pseudopotential approach to DFT as implemented within the VASP code [28] using PAW potentials[29, 30]. (The Tb potential does not have  $f$  electrons in the valence.) We use the local-density approximation (Ceperley-Alder[31] with Vosko-Wilk-Nusair correlation[32]) with on-site Coulomb interactions (LDA+U). We let  $U=1$  eV to make the band gap close to the experimental value of  $\sim 0.5$  eV [33]. Since the first-principles calculations require periodic boundary conditions, we study a system in which the cycloidal spin structure is commensurate with  $k_s = 1/3$ , making a supercell that is tripled in  $b$ -direction (60 atoms per cell) as shown in Fig.1. This is close enough to the experimental  $k_s$  of 0.28 that our results can be expected to be qualitatively and semiquantitatively meaningful. A  $3 \times 1 \times 2$   $k$ -point sampling is used. The plane-wave energy cutoff was 500 eV, and the electric polarization was calculated using the Berry-phase approach [34].

A structural relaxation was performed for the 60-atom supercell without SO. The resulting structural coordinates, reported in Table I, are in quite satisfactory agreement with experiment. Our computed magnetic moments have magnitudes  $3.4 \mu_B$  and rotate in the  $b-c$  plane as one scans along  $b$ , and this result hardly changes when SO is turned on. Experimentally, the magnetic moments on  $\text{Mn}^{3+}$  sites are found to form an elliptical spiral with amplitudes  $m_b = 3.9 \mu_B$  and  $m_c = 2.8 \mu_B$  [13]. The origin of this ellipticity, which is apparently not captured by our calculation, deserves further investigation.

Next, we confirmed that the Berry-phase polarization vanishes in the absence of SO. When the SO is turned on, one expects the broken inversion symmetry in the spin sector to be communicated to the spatial (charge) degrees of freedom, and indeed our calculations confirm this. Focusing first on the purely electronic mechanism, we froze the lattice vectors and ionic positions while turning on the SOI and computed the polarization to be  $P = 32 \mu\text{C}/\text{m}^2$  along the  $c$  direction[36] (and zero along directions  $a$  and  $b$ ). This is much smaller than the experimental value of  $\sim 600 \mu\text{C}/\text{m}^2$  [12], suggesting that the

TABLE I: Experimental (Ref. 35) and theoretical (this work) structural parameters for orthorhombic  $\text{TbMnO}_3$ .

		Experiment	Theory
Lattice vectors		$a$ ( $\text{\AA}$ )	5.293
		$b$ ( $\text{\AA}$ )	5.838
		$c$ ( $\text{\AA}$ )	7.403
Tb	$4c(x y 1/4)$	$x$	0.983
		$y$	0.082
Mn	$4b(1/2 0 0)$	$x$	0.104
		$y$	0.467
O1	$4c(x y 1/4)$	$x$	0.704
		$y$	0.326
		$z$	0.051
O2	$8d(x y z)$	$x$	0.699
		$y$	0.320
		$z$	0.052

lattice mechanism must be dominant. We thus turned our attention next to the role of ionic displacements.

As a first step, we computed the Hellmann-Feynman forces appearing on the ions as the SO is turned on (with the structural coordinates still clamped). Using the 20-atom cell of the  $Pbnm$  space group to label the forces, we found that: (i) 64.8% of the forces belong to the symmetry-preserving  $A_1(\Gamma)$  irreducible representation (irrep); (ii) 28.7% of the forces belong to the  $B_{3u}(\Gamma)$  irrep, i.e., zone-center infrared-active (IR-active) modes with dynamical dipoles along  $c$ ; and (iii) 6.5% correspond to forces at  $k_y = \pm 2\pi/3b$ , i.e., those that would be responsible for lowering the translational symmetry of the 20-atom cell. The remaining contributions are found to vanish to numerical precision. Since the only forces that generate an electric polarization in linear order are those of type (ii), we henceforth focus our attention on the zone-center IR-active  $B_{3u}$  modes.

Eight Wyckoff coordinates contribute to the  $B_{3u}$  irrep in the 20-atom  $Pbnm$  structure: three associated with Mn atoms in Wyckoff position 4b, one each for Tb and O1 atoms in Wyckoff position 4c, and three for the O2 atoms in Wyckoff position 8d [37]. To find the polarization induced by the SOI, we need to deduce the displacements resulting from these forces. To this end we calculated the  $8 \times 8$  force-constant matrix  $\Phi_{ij} = -\partial f_i / \partial u_j$  connecting the  $B_{3u}$  forces and displacements at linear order using finite-difference methods (i.e., we shift each Wyckoff coordinate by  $\sim 10^{-3} \text{\AA}$  and calculate the resulting forces). For computational convenience, the determination of  $\Phi_{ij}$  was done in the absence of SO. (We checked a few elements and found hardly any difference in the presence of SO [38].) Furthermore, we identify the linear combination  $t_j$  of the eight coordinates corresponding to a uniform shift of the crystal along the  $c$  direction (acoustic mode) and make sure to project this combination out of the computed forces and displacements. Thus, the displacements are predicted from  $u_i = -\sum_{j=1}^8 \tilde{\Phi}_{ij}^{-1} f_j$ , where  $\tilde{\Phi}^{-1}$  is a pseudo-inverse [39] having the properties that  $\tilde{\Phi}^{-1} \Phi u = u$  for any  $u$  orthogonal to  $t$ .

TABLE II: Forces, displacements, effective charges and contributions to ionic polarization from IR-active  $B_{3u}$  modes.

Wyckoff coordinate	$F$ (meV/Å)	$\Delta u$ (mÅ)	$Z^*$ (e)	$\Delta P$ ( $\mu\text{C}/\text{m}^2$ )
1 (Tb 4c, $z$ )	0.434	-0.171	7.468	-94
2 (O1 4c, $z$ )	2.264	-0.162	-6.815	81
3 (Mn 4b, $x$ )	-7.039	-0.315	0.567	-13
4 (Mn 4b, $z$ )	-8.933	-0.453	7.460	-248
5 (Mn 4b, $y$ )	-2.940	-0.012	0.553	-0.5
6 (O2 8d, $x$ )	5.058	0.540	0.077	3
7 (O2 8d, $y$ )	3.573	0.934	0.227	16
8 (O2 8d, $z$ )	4.409	0.556	-5.738	-234

The computed forces and predicted atomic displacements in the IR-active  $B_{3u}$  sector for  $\text{TbMnO}_3$  are presented in the first three columns of Table II. We calculated the  $B_{3u}(\Gamma)$  forces again in the presence of the predicted displacements and found that 99% of these forces were eliminated, thus justifying our approach [40]. The distorted crystal structure is now non-centrosymmetric (space group  $Pna2_1$ ), and the calculated Berry-phase polarization (including both electronic and ionic contributions) is  $P = -467 \mu\text{C}/\text{m}^2$ . This is more than an order of magnitude larger than the value of  $32 \mu\text{C}/\text{m}^2$  computed from purely electronic mechanisms, and comparable in magnitude with the experimental value of  $\sim -600 \mu\text{C}/\text{m}^2$  [14]. Note that the sign of the ionic contribution is different from the purely electronic contribution, making the sign of the total polarization consistent with experiment. We thus arrive at the first major conclusion of our paper, namely, that the lattice contributions dominate strongly and have approximately the right magnitude to explain the experimentally observed polarization. Purely electronic mechanisms, e.g. as described by the Katsura-Nagaosa-Balatsky (KNB) model[18] or related work [19, 20, 21], are not sufficient to describe the ferroelectricity in  $\text{TbMnO}_3$ .

We focus henceforth on the lattice-mediated contribution to the polarization. To understand which modes contribute most strongly and to test whether simple models (based, e.g., on DM interactions) can predict the forces and displacements, we performed a further analysis as follows. For each  $B_{3u}$  Wyckoff coordinate, we computed the corresponding effective charge  $Z^*$  (derivative of polarization with respect to the Wyckoff coordinate) by augmenting the same finite-difference calculations used earlier with Berry-phase polarization calculations. We then multiplied effective charges and displacements to get the contribution  $\Delta P$  made by each Wyckoff coordinate. The results are given in the last two columns of Table II. The total ionic polarization (sum of the last column) is  $-489 \mu\text{C}/\text{m}^2$ , in good agreement with the change of polarization in going from the centrosymmetric to the distorted structure as reported earlier ( $-467 - 32 = -499 \mu\text{C}/\text{m}^2$ ). Not surprisingly, the  $Z^*$

TABLE III: Forces, displacements, effective charges and contributions to ionic polarization from modes corresponding to eigenvectors of the force-constant matrix.

Eigenvalue (eV/Å <sup>2</sup> )	$F$ (meV/Å)	$\Delta u$ (mÅ)	$Z^*$ (e)	$\Delta P$ ( $\mu\text{C}/\text{m}^2$ )
34.86	6.349	0.182	-8.111	-108
31.37	-8.259	-0.263	4.565	-88
13.32	2.783	0.209	8.132	125
11.87	7.614	0.641	-2.127	-100
10.35	1.684	0.163	-3.406	-41
6.99	-2.784	-0.398	4.316	-126
3.85	4.032	1.047	-1.991	-153

values are much larger for the four Wyckoff coordinates involving displacements along  $z$ , and the corresponding  $\Delta P$  values give by far the largest contribution.

In a simple DM model [5], one considers interactions involving nearest-neighbor triplets of ions along Mn–O–Mn bonds. Such a picture leads to the expectation that a force  $\gamma \hat{\mathbf{e}}_{nn'} \times \mathbf{S}_n \times \mathbf{S}_{n'}$  should appear on the central O ion (where  $\gamma$  is a coupling,  $\mathbf{S}_n$  and  $\mathbf{S}_{n'}$  are neighboring Mn spins, and  $\hat{\mathbf{e}}_{nn'}$  is the unit vector connecting them), with an equal and opposite force shared between the Mn ions. The cycloidal spin structure of  $\text{TbMnO}_3$  is such that O1 ions should be unaffected, and O2 ions should all feel the same force along  $c$ , with Mn ions feeling an opposite force. Thus, within such a model one would expect only the 4th and 8th rows of Table II to give significant contributions. Inspecting the Table, we see that this is rather far from being the case; one does find substantial oppositely-directed forces and displacements for the (Mn 4b,  $z$ ) and (O2 8d,  $z$ ) coordinates, but the forces and displacements are comparable for some other coordinates. The contributions to  $\Delta P$  are more strongly dominated by these two coordinates, but only because the  $Z^*$  values are so much larger for displacements along  $\hat{z}$ . Interestingly, the Tb displacements are responsible for  $\sim 20\%$  of the lattice polarization, despite being uninvolved in the usual picture of Mn–O–Mn couplings. Thus we conclude that the simple DM model, and indeed any model that considers only nearest-neighbor Mn–Mn spin interactions, is unable to provide a detailed description of the ferroelectricity in  $\text{TbMnO}_3$ .

As an alternative way of analyzing the SO-induced  $B_{3u}$  forces and displacements, we transform into the basis of eigenvectors of the  $8 \times 8$  force-constant matrix  $\Phi$ . The results are presented in Table III. (Components on the translational zero mode, not shown in the Table, were numerically negligible.) We find that the forces are rather widely distributed among these “modes.” Not surprisingly, the displacements are largest for the softest mode, but other modes also show substantial displacements. Moreover, the mode dynamical charges are much larger for some of the harder modes, with the result that the contributions to the polarization are of comparable mag-

nitude for almost all of the  $B_{3u}$  modes. Thus, it is clear that the physics of the electric polarization in  $TbMnO_3$  is not dominated by a single softest mode.

To investigate the role of spin-orbit effects located on the various atomic sites, we performed additional calculations of the forces (and, via the force-constant matrix, the resulting lattice polarizations). We first turned the SOI off on all sites other than Tb, then Mn, then O, finding contributions to the polarization of  $-11 \mu C/m^2$ ,  $-447 \mu C/m^2$  and  $-8 \mu C/m^2$ , respectively. (The sum is in fairly good agreement with the total ionic polarization of  $-489 \mu C/m^2$ ; this and other tests confirm that the results are roughly linear in SO coupling.) This confirms that the SOI on the Mn sites is responsible for almost all of the lattice-mediated contribution to the polarization, even though some of these forces appear on other sites, even including Tb (see Table II).

Up to now our analysis has been done using the 60-atom supercell, whose cycloidal wavevector ( $k_s=1/3$ ) approximates the experimental one ( $k_s=0.28$ ). To investigate how the results depend on  $k_s$ , we have also carried calculations of the SO-induced forces for a 40-atom supercell ( $k_s=1/2$ ). In order to isolate the effects of the spin-wave period, we calculated the forces at the same structural coordinates as for the 60-atom structure, and again projected into the  $B_{3u}(\Gamma)$  irrep. We find that the pattern of  $B_{3u}$  forces matches almost exactly that of the 60-atom cell (with the angle between the two eight-dimensional vectors being  $\sim 3^\circ$ ), although the magnitude is larger for the 40-atom cell. From the simple DM model one expects  $\mathbf{P} \propto \mathbf{e}_{n,n'} \times (\mathbf{S}_n \times \mathbf{S}_{n'})$  [9] where the spins are neighbors on the zig-zag chains propagating along  $b$  (see Fig. 1). The angle between the spins is  $90^\circ$  and  $60^\circ$  for the 40-atom and 60-atom supercells respectively, giving an expected ratio of  $2 : \sqrt{3}=1.15$ . In the long-wavelength limit one expects  $\mathbf{P} \propto |k_s|$ , for a ratio of 1.5. Strangely, our computed ratio for the 40- and 60-atom supercells is about 1.48, closer to the continuum expression in spite of the rather short wavelength of the spiral. This may be another indication that further-neighbor Mn-Mn interactions, or other effects not captured by a nearest-neighbor DM model, play an important role. From the forces we predict a lattice polarization of  $-754 \mu C/m^2$  for  $k_s=1/2$ ; extrapolating through our  $k_s=1/3$  result, we estimate a lattice polarization of  $-410 \mu C/m^2$  for  $k_s=0.28$ .

In summary, we have used first-principles methods to compute the electronic and lattice contributions to the spin-orbit induced electric polarization in the cycloidal-spin compound  $TbMnO_3$ , and find the lattice contribution to be strongly dominant. We provide a detailed analysis of the lattice contributions coming from individual sites and individual modes and roughly characterize the dependence of the lattice polarization on spin-wave period. Our result for the polarization agrees in sign and compares fairly well in magnitude with the experimentally measured value of  $\sim -600 \mu C/m^2$  [14].

The authors wish to thank Morrel H. Cohen and Craig J. Fennie for fruitful discussions. This work was supported by NSF Grant No. DMR-0549198.

*Note:* While finalizing this manuscript, we learned of closely related work by H.J. Xiang *et al.* [41]

- 
- \* Electronic address: andreim@physics.rutgers.edu
- [1] M. Fiebig, J. Phys. D: Appl. Phys. **38**, R123 (2005).
  - [2] L. C. Chapon *et al.*, Phys. Rev. Lett. **93**, 177402 (2004).
  - [3] L. C. Chapon, P. G. Radaelli, G. R. Blake, S. Park, and S. W. Cheong, Phys. Rev. Lett. **96**, 097601 (2006).
  - [4] A. Munoz *et al.*, Inorg. Chem. **40**, 1020 (2001).
  - [5] I. A. Sergienko, C. Sen, and E. Dagotto, Phys. Rev. Lett. **97**, 227204 (2006).
  - [6] N. Aliouane *et al.*, Phys. Rev. B **73**, 020102(R) (2006).
  - [7] Y. J. Choi *et al.*, Phys. Rev. Lett. **100**, 047601 (2008).
  - [8] S.-W. Cheong and M. Mostovoy, Nature Materials **6**, 13 (2007).
  - [9] T. Kimura, Annu. Rev. Matter. Res. **37**, 387 (2007).
  - [10] G. Lawes *et al.*, Phys. Rev. Lett. **95**, 087205 (2005).
  - [11] T. Kimura, J. C. Lashley, and A. P. Ramirez, Phys. Rev. B **73**, 220401(R) (2006).
  - [12] T. Kimura *et al.*, Nature **426**, 55 (2003).
  - [13] M. Kenzelmann *et al.*, Phys. Rev. Lett. **95**, 087206 (2005).
  - [14] Y. Yamasaki *et al.*, Phys. Rev. Lett **98**, 147204 (2007); *ibid.*, to be published (erratum).
  - [15] M. Mostovoy, Phys. Rev. Lett. **96**, 067601 (2006).
  - [16] P. G. Radaelli and L. C. Chapon, Phys. Rev. B **76**, 054428 (2007).
  - [17] A. B. Harris, J. Appl. Phys. **99**, 08E303 (2006).
  - [18] H. Katsura, N. Nagaosa, and A. V. Balatsky, Phys. Rev. Lett. **95**, 057205 (2005).
  - [19] P. Bruno and V. K. Dugaev, Phys. Rev. B **72**, 241302(R) (2005).
  - [20] C. Jia, S. Onoda, N. Nagaosa, and J. H. Han, Phys. Rev. B **74**, 224444 (2006).
  - [21] C. Jia, S. Onoda, N. Nagaosa, and J. H. Han, Phys. Rev. B **76**, 144424 (2007).
  - [22] I. A. Sergienko and E. Dagotto, Phys. Rev. B **73**, 094434 (2006).
  - [23] C. D. Hu, <http://arxiv.org/abs/0711.0100v1>.
  - [24] N. A. Hill, Annu. Rev. Mater. Res. **32**, 1 (2002).
  - [25] C. Wang, G.-C. Guo, and L. He, Phys. Rev. Lett. **99**, 177202 (2007).
  - [26] S. Picozzi, K. Yamauchi, B. Sanyal, I. A. Sergienko, and E. Dagotto, Phys. Rev. Lett. **99**, 227201 (2007).
  - [27] H. J. Xiang and M.-H. Whangbo, Phys. Rev. Lett. **99**, 257203 (2007).
  - [28] G. Kresse and J. Furthmüller, Comput. Mater. Sci. **6**, 15 (1996); Phys. Rev. B **54**, 11169 (1996).
  - [29] P. E. Blöchl, Phys. Rev. B **50**, 17953 (1994).
  - [30] G. Kresse and D. Joubert, Phys. Rev. B **59**, 1758 (1999).
  - [31] D. M. Ceperley and B. J. Alder, Phys. Rev. Lett. **45**, 566 (1980).
  - [32] S. H. Vosko, L. Wilk, and M. Nusair, Can. J. Phys. **58**, 1200 (1980).
  - [33] Y. Cui, C. Wang, and B. Cao, Solid State Communications **133**, 641 (2005).
  - [34] R. D. King-Smith and D. Vanderbilt, Phys. Rev. B **47**,

- 1651 (1993).
- [35] J. Alonso et al., *Inorg. Chem.* **39**, 917 (2000).
- [36] The uncertainty in the calculated values of polarization is estimated to be of the order of 5-10  $\mu\text{C}/\text{m}^2$ .
- [37] E. Kroumova et al., *Phase Transitions* **76**, 155 (2003).
- [38] In any case, a dependence of  $\Phi_{ij}$  on SOI would only give a dependence of polarization at quadratic or higher order. We are primarily concerned with linear effects.
- [39] X. Wu, D. Vanderbilt, and D. R. Hamann, *Phys. Rev. B* **72**, 035105 (2005).
- [40] One could alternatively just relax the atomic coordinates in the presence of SOI. However, we prefer the present approach because it is numerically more stable, it facilitates analysis of distortions and polarizations in terms of phonon modes, and it allows for efficient testing of various effects (e.g., turning off the SOI on certain sites) without the need to perform additional ionic relaxations.
- [41] H. J. Xiang et al. (2008), <http://arxiv.org/abs/0803.2741>.